

# Theory of Flying-Adder Frequency Synthesizers—Part II: Time- and Frequency-Domain Properties of the Output Signal

Paul P. Sotiriadis, *Senior Member, IEEE*

**Abstract**—This is a rigorous mathematical theory of the operation of the flying-adder (FA) frequency synthesizer (also called direct digital period synthesizer). The paper consists of two parts. Part I presents a detailed mathematical model of the FA synthesizer, capturing the relationships between the properties of the FA's output and internal signals and the FA's parameters. The counting of the rising edges in the FA's multiplexer's output establishes a discrete-time index that is used to analytically derive the fundamental discrete-time periods of all the FA's signals. The continuous-time intervals between the rising edges are calculated and used to derive the fundamental continuous-time periods of the signals from the corresponding discrete-time ones. It is shown that the FA behaves differently within different ranges of the frequency word, and the practically useful range is identified. The FA's output average frequency, along with its maximum and minimum values, is analytically derived by calculating the number of cycles in the output signal within a fundamental continuous-time period of it. The relationship between the average and the fundamental output frequencies is also established, indicating the potential frequencies and density of output spurious frequency components. Part II of the paper characterizes the timing structure of the output signal, providing analytical expressions of the pulses' locations, analytical strict bounds of the timing irregularities, and exact analytical expressions of several standard jitter metrics. Spectral properties of the output waveform are presented, including the dominance of the frequency component at the average frequency, and analytical expressions of the dc value and average power of the output signal are derived. The FA has been implemented in a Xilinx Spartan-3E field-programmable gate array, and spectral measurements are presented, confirming the theoretical results. Extensive MATLAB simulation has also been used to generate numerous examples, illustrating the developed theory.

**Index Terms**—Clock generation, digital-to-frequency converter (DFC), direct digital period synthesis, direct digital synthesis (DDS), flying adder (FA), frequency synthesis, jitter, phase accumulator, phase synthesis, spurs, truncation.

## I. INTRODUCTION

THIS is the second part of a two-part paper [1] presenting a rigorous mathematical theory of the operation of flying-adder (FA) frequency synthesizers.

Manuscript received March 07, 2009; revised July 20, 2009; accepted October 02, 2009. Date of publication March 29, 2010; date of current version August 11, 2010. This paper was recommended by Associate Editor A. Strollo.

The author is with Sotekco LLC, Baltimore, MD 21201-2404 USA (e-mail: pps@ieee.org).

Digital Object Identifier 10.1109/TCSI.2009.2039835

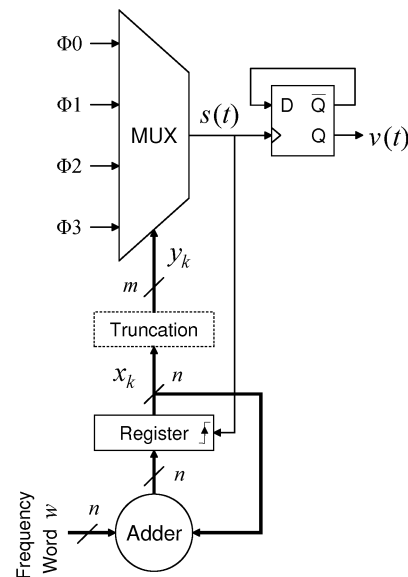


Fig. 1. FA (shown here with  $m = 2$ , i.e.,  $2^m$  input phases).

The FA [2], [3], which is also referred to as direct digital period synthesizer [4] or digital-to-frequency converter (DFC), [5], appeared as an independent frequency synthesis architecture<sup>1</sup> in [2] and as a patented invention in [3], followed by a number of related publications, including [4]–[20]. The FA shares some functionality with circuits that involve phase-switching prescalers and digital phase accumulators and have been used in the past [21]–[28] as well as in more recent architectures [29], [30].

The FA, in abstract form, is shown in Fig. 1. It is driven by a family of uniformly phase-shifted copies of a frequency reference clock. The FA is a simple fully digital frequency synthesizer with good period (frequency) resolution and range. These qualities make FA a very useful circuit for clocking digital circuits that can tolerate a certain amount of deterministic jitter. Regarding analog and RF circuit applications, the FA suffers from highly spurious output content (for most frequency words) due to phase truncation, and research effort has been devoted in estimating this spurious content [10], [12], [17].

The FA's output signal resembles that of the pulse-output direct digital synthesizer (PDDS) [24], although the FA's internal structure is significantly different from that of PDDS because

<sup>1</sup>To the best of the author's knowledge.

its register is updated at a variable rate. This makes the analysis of the FA's operation different, yet similar in nature, to that of DDS, which has been studied extensively in [24], [26], [27], [31]–[41], and many other publications.

For most parameter values, the output signal is a periodic juxtaposition of cycles of two possible lengths. This results in timing irregularity of the output signal in the time domain and in spurious frequency components in the output spectrum, which both may impact the operation of any circuit clocked by the FA.

Part II of the paper studies in detail the timing of the pulses in the output signal of the FA and relates the periodicity of the FA's signals to qualitative properties of its output spectrum. Part II builds on the mathematical model of the FA introduced and the fundamental discrete-time and continuous-time periods of the FA's signals derived in Part I [1].

Compact closed-form expressions are derived for the position (beginning and ending) of the output pulses. The possible output waveform types are analyzed and classified based on the FA parameters. The lengths of the 0 and 1 intervals are derived, and exact analytical expressions of the absolute, absolute cycle-to-cycle, accumulated, cycle-average, and cycle-to-cycle average jitter metrics are provided.

In addition, analytical expressions are derived for the output average voltage (dc), the output average power, and bounds of the power of the frequency component at the output average frequency  $f_{av}$  [5]. Moreover, the dominance of the signal component at frequency  $f_{av}$  is proven under certain conditions on the FA parameters.

Section II expands the FA's model in Part I by introducing the additional notation and variables used here. Section III derives the positions of the output pulses and the lengths of the 0 and 1 intervals and classifies the possible types of output waveforms based on the FA parameters. Section IV derives analytical expressions of several standard jitter metrics. Section V derives analytical expressions of the output average voltage, the average power, and the dc power. It provides bounds of the power of the frequency component at the output average frequency and its dominance under certain conditions on the FA parameters. Finally, Section VI connects the findings of all the previous sections and the findings in [1] with qualitative spectral properties of the FA's output signal derived by measurements and simulation.

## II. MODEL SUMMARY AND ADDITIONS

The model, notation, and operation of the FA in Fig. 1 is presented in detail in [1, Sec. 2]. The FA is driven by the family  $\phi_1, \phi_2, \dots, \phi_{2^m-1}$  of  $2^m$  periodic square-wave 50% duty-cycle (clock) signals of the same frequency  $f_{clk} = 1/T$  and relative phase offsets that form an arithmetic progression with step of  $-2\pi/2^m$  radians corresponding to time offset  $\Delta = T/2^m$ .

The main parameters of the FA used in this second part of the paper [1] are summarized following Fig. 1.

The *discrete-time* reference variable  $k$  is the counter of the rising edges in signal  $s$  at the output of the MUX. We refer to the (real) continuous-time interval between the  $k$ th and the  $k+1$  rising edges as the  $k$ th discrete-time interval.

The *modified difference sequence*  $\{\delta_k\}$  is defined such that  $\delta_k\Delta$  is the length of the  $k$ th discrete-time interval.

The *fundamental discrete-time period* of  $\{\delta_k\}$  is  $L$ , as given by [1, eq. (10)]. The *fundamental continuous-time period*<sup>2</sup> of  $\{\delta_k\}$  is  $T_p$ , as given by [1, eq. (24)].

The rising and falling edges of the output signal  $v$  appear at the time moments  $t_\ell$ ,  $\ell = 1, 2, 3, \dots$ , and  $\tau_\ell$ ,  $\ell = 1, 2, 3, \dots$ , respectively.

The (real) continuous-time period of the output  $v$  is  $T_v$ , as given by [1, eq. (34)].

The *average frequency*  $f_{av}$  of the output signal  $v$ , which is defined as the number of cycles within a *fundamental continuous-time period*<sup>2</sup>  $T_v$ , divided by  $T_v$ , is given by [1, eq. (36)].

The frequency  $f_{av}$  is the  $N_{av}$  harmonic of the *fundamental frequency*  $f_{vf} = 1/T_v$  of  $v$ , i.e.,  $f_{av} = N_{av}f_{vf}$ , where  $N_{av}$  is given by [1, eq. (42)]

### A. Additional Notation

This section lists the definitions of variables and parameters used here that have *not* been introduced in [1].

- $D_C$ : *Duty cycle* of the output signal  $v$  defined *only* in the special case that  $v$  is a juxtaposition of identical cycles.
- $\tilde{t}_j, \tilde{\tau}_j$ : The continuous-time moments at which the  $j$ th rising and falling edges, respectively, appear of the ideal 50% duty-cycle square wave of frequency  $f_{av}$ , whose first rising edge coincides with that of  $v$ .
- $T_{av}$ : The *average frequency period* of the output signal  $v(t)$  is equal to  $T_{av} = 1/f_{av}$  and can alternatively be defined as the ratio of  $T_v$  to the number of pulses of  $v$  within  $T_v$ .
- $\bar{v}$ : The *output average voltage* is the mean value of  $v(t)$  within a fundamental continuous-time period  $T_v$  of it.
- $P$ : The *output average power* is the mean power of  $v(t)$  within a fundamental continuous-time period  $T_v$  of it.
- $P_0$ : The *output dc power* is the power of the dc component of  $v(t)$ .
- $P_{L/2}$ : The *power of the  $L/2$  harmonic* of the output signal  $v(t)$ . Note that the  $L/2$  harmonic frequency is equal to  $f_{av}$  when  $L > 1$  (see [1, eq. (10)] and [1, Corollary 5.3]).
- $R_P$ : The *power ratio* of  $P_{L/2}$  to the total power of the rest of the harmonics, except the dc.

## III. LENGTHS AND TIMING OF PULSES AND CYCLES IN THE OUTPUT SIGNAL $v$

This section examines the timing irregularities in  $v$ . It provides tight bounds of the length of the individual cycles, the lengths of the 0 and 1 intervals (see definition below), as well as the duty cycle of the individual cycles in  $v$ .

The output signal  $v$  has average frequency  $f_{av}$ , which is given by [1, eq. (36)], in the sense of the number of pulses per period  $T_v$ . The timing of pulses however can be irregular. Consider, for example, the waveforms of  $v(t)$  in [1, Fig. 3(g)] and [1, Fig. 5(g)], where the time intervals between consecutive pulses vary, and the cycles have unequal lengths. In other cases, the cycles are identical but the duty cycle is not 50%.

Observe in [1, Fig. 4(g)] that  $v(t)$  is a highly irregular signal (compared with the ideal periodic square wave). Following the remarks in [1, Example 2.2], one can conclude that this is the

<sup>2</sup>All continuous-time intervals and periods we consider start and end at a rising edge (or a spike) of signal  $s(t)$ . Note that every rising edge and spike of  $s(t)$  appear at continuous time  $t = r\Delta$  for some nonnegative integer  $r$ .

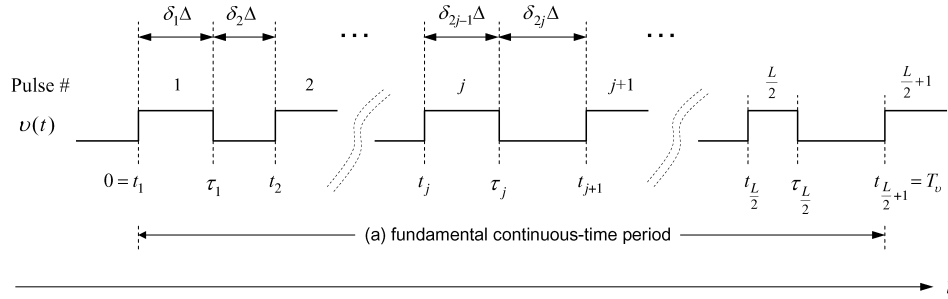


Fig. 2. Timing of the pulses in  $v(t)$  within a fundamental continuous-time period  $T_v$  when  $L > 1$  and assuming the initial conditions  $x_0 = 0$  and  $v(0^-) = 0$ , i.e., D-FF being reset at  $t = 0^-$ , which imply that the first pulse starts at  $t = t_1 = 0$ .

most typical case when  $0 < w < 2^{n-m}$ . Since such signals do not resemble the ideal periodic square wave at all,<sup>3</sup> we exclude them from the analysis in this section.

**Throughout this section, we assume that  $2^{n-m} \leq w < 2^n$ .**

In the time-domain, deviation from the ideal square-wave periodic signal results in “deterministic jitter.” In the frequency domain, it introduces (some of) the harmonic frequencies  $qf_{v_f}$ ,  $q = 0, 1, 2, \dots$ , in the output spectrum, where  $f_{v_f} = 1/T_v$ , in addition to the average frequency  $f_{av} = N_{av}f_{v_f}$  of  $v$ .

*Definition 3.1:* A 1-interval  $(t_a, t_b)$  is a continuous-time interval such that  $v(t) = 1$  for all  $t \in (t_a, t_b)$  and  $v(t_a^-) = v(t_b^+) = 0$ . Pulse is another name for the 1 intervals. The 0 interval is defined accordingly. By the definition of  $\{\delta_k\}$ , the length of the  $k$ th (0- or 1-) interval is  $\delta_k\Delta$  seconds. A cycle is a pair of 0 and 1 consecutive intervals in any of the orders 0–1 or 1–0.

For presentation convenience, we assume the initial conditions  $x_0 = 0$  and  $v(0^-) = 0$ , i.e., D-FF being reset at  $t = 0^-$ , which imply that the first pulse starts at  $t = t_1 = 0$ . In this case, the output waveform is shown in Fig. 2, illustrating the above definitions (it is convenient to focus on the 1–0 cycles).

Fig. 2 shows  $L/2$  1–0 cycles and  $L/2$  pulses within the period  $T_v$ . This is the case when  $L > 1$ , resulting from [1, Corollary 5.3]. As shown in Theorem 3.1 below, the case  $L = 1$  is trivial.

Note that the  $j$ th 1–0 cycle, in the fundamental continuous-time period starting at  $t = 0$ , is  $t_{j+1} - t_j = (\delta_{2j-1} + \delta_{2j})\Delta$  seconds long. In addition, the length of the  $j$ th pulse is  $\tau_j - t_j = \delta_{2j-1}\Delta$  seconds.

### A. Pulse Widths and Cycle Lengths

The following theorem gives some insight in the properties of the individual pulses and cycles in  $v$ .

*Theorem 3.1:* If  $2^{n-m} \leq w < 2^n$ , then we have the following:

- A) If  $L = 1$ , i.e., if  $2^{n-m}$  divides  $w$ , then  $v$  is the ideal 50% duty-cycle square wave, and every pulse of  $v$  corresponds to two consecutive rising edges of  $s$ . In addition, from [1, eq. (34)], the length of the cycles is

$$T_v = \frac{w}{2^{n-m-1}}\Delta. \tag{1}$$

<sup>3</sup>Although they may be very useful in certain applications requiring periodic waveforms with rich spectrum.

- B) If<sup>4</sup>  $L = 2$ , i.e.,  $\text{gcd}(w, 2^{n-m}) = 2^{n-m-1}$ , then all cycles<sup>5</sup> of  $v$  are identical with length equal to

$$T_v = T_p = \frac{w}{2^{n-m-1}}\Delta \tag{2}$$

and duty cycle

$$D_c = \frac{1}{2} \left[ \frac{w}{2^{n-m}} \right] \frac{2^{n-m}}{w} \tag{3}$$

(assuming that  $x_0 = 0$  and the D-FF is initially reset, i.e.,  $v(0^-) = 0$ ; it may be  $1 - D_c$  under other initial conditions). Again, every pulse of  $v$  corresponds to two consecutive rising edges of  $s$ .

- C) If  $L > 2$ , i.e.,  $w$  is not a multiple of  $2^{n-m-1}$ , then the length of every 0 and 1 interval in  $v$  is equal to one of the two values

$$\left[ \frac{w}{2^{n-m}} \right] \Delta, \quad \left( \left[ \frac{w}{2^{n-m}} \right] + 1 \right) \Delta. \tag{4}$$

Moreover, within every fundamental continuous-time period<sup>6</sup>  $T_v$  of  $v$ , there exist at least two intervals (0 or 1 or both), one of length equal to the lower value in (4) and one of length equal to the higher value in (4). Finally, the length of every cycle (1–0 or 0–1) can only take one of the two values

$$\left[ \frac{2w}{2^{n-m}} \right] \Delta, \quad \left( \left[ \frac{2w}{2^{n-m}} \right] + 1 \right) \Delta \tag{5}$$

and within every two consecutive fundamental continuous-time periods  $T_v$  of  $v$  (or one fundamental period extended by one interval) there exist at least one 1–0 and one 0–1 cycles of length equal to the lower value in (5) and at least one 1–0 and one 0–1 cycles of length equal to the higher value in (5).

*Example 3.1:* Consider [1, Example 2.1] and [1, Fig. 3(f) and (g)]. Using [1, eq. (10)] and [1, eq. (34)], we derive  $L = 4$  and  $T_v = 7\Delta$ . A continuous-time fundamental period of  $v(t)$  is shown in [1, Fig. 3(g)] between  $t = 0$  and  $t = 7\Delta$ . Observe that the two 1 intervals have lengths  $\Delta$  and  $2\Delta$ ; also, the two 1–0

<sup>4</sup>For  $L$  to be equal to 2, it is necessary that  $n \geq m + 1$ .

<sup>5</sup>It is convenient to consider only 1–0 cycles here.

<sup>6</sup>All continuous-time periods and intervals we consider begin and end at a rising edge (or spike) of signal  $s(t)$ .

cycles have lengths  $3\Delta$  and  $4\Delta$ . Referring to Theorem 3.1, we have  $L = 4$  and

$$\left\lceil \frac{w}{2^{n-m}} \right\rceil = \left\lceil \frac{7}{4} \right\rceil = 1$$

which imply that  $\delta_k \in \{1, 2\}$ , and both values are taken by  $\delta_k$ . Therefore, the theorem is in agreement with the example. Moreover, it is

$$\left\lceil \frac{2w}{2^{n-m}} \right\rceil = \left\lceil \frac{14}{4} \right\rceil = 3$$

and Theorem 3.1 implies that  $\delta_k + \delta_{k+1} \in \{3, 4\}$ , and both values are taken by  $\delta_k + \delta_{k+1}$ . Again, the theorem fully agrees with the observations in [1, Fig. 3(f) and (g)].

*Example 3.2:* Consider [1, Example 2.3] and [1, Fig. 5(f) and (g)]. It is  $L = 4$  and  $T_v = 15\Delta$ . A continuous-time fundamental period of  $v(t)$  is shown between  $t = 0$  and  $t = 15\Delta$ . Observe that the two 1 intervals have lengths  $3\Delta$  and  $4\Delta$ ; the two 1-0 cycles have lengths  $7\Delta$  and  $8\Delta$ . Theorem 3.1 implies that  $\delta_k \in \{3, 4\}$ , with both values taken, and  $\delta_k + \delta_{k+1} \in \{7, 8\}$ , with both values taken as well. Again, these fully agree with the observations in [1, Fig. 5(f) and (g)].

*Proof (of Theorem 3.1):* Fact 1 in the Appendix implies

$$\left\lceil \frac{w}{2^{n-m}} \right\rceil \leq \left\lceil \frac{kw}{2^{n-m}} \right\rceil - \left\lceil \frac{(k-1)w}{2^{n-m}} \right\rceil \leq \left\lceil \frac{w}{2^{n-m}} \right\rceil \quad (6)$$

where  $\lceil \cdot \rceil$  is the ceiling function. In addition, our assumption  $2^{n-m} \leq w < 2^n$  implies

$$1 \leq \left\lceil \frac{w}{2^{n-m}} \right\rceil \quad \text{and} \quad \left\lceil \frac{w}{2^{n-m}} \right\rceil \leq 2^m$$

which along with (6) gives

$$1 \leq \left\lceil \frac{kw}{2^{n-m}} \right\rceil - \left\lceil \frac{(k-1)w}{2^{n-m}} \right\rceil \leq 2^m. \quad (7)$$

From (7), the definition of  $\delta_k$ , and the two equations [1, eqs. (4) and (5)], we get

$$\delta_k = \left\lceil \frac{kw}{2^{n-m}} \right\rceil - \left\lceil \frac{(k-1)w}{2^{n-m}} \right\rceil \quad (8)$$

which combined with (6) implies

$$\left\lceil \frac{w}{2^{n-m}} \right\rceil \leq \delta_k \leq \left\lceil \frac{w}{2^{n-m}} \right\rceil$$

and since the upper and lower bounds are either identical or consecutive positive integers, it is<sup>7</sup>

$$\delta_k \in \left\{ \left\lceil \frac{w}{2^{n-m}} \right\rceil, \left\lceil \frac{w}{2^{n-m}} \right\rceil + 1 \right\}. \quad (9)$$

Using (8) twice, we get

$$\delta_k + \delta_{k+1} = \left\lceil \frac{(k+1)w}{2^{n-m}} \right\rceil - \left\lceil \frac{(k-1)w}{2^{n-m}} \right\rceil$$

<sup>7</sup>With the understanding that if both numbers in the set (9) are the same, we ignore one to comply with the standard definition of sets.

which along with Fact 1 in Appendix gives

$$\left\lceil \frac{2w}{2^{n-m}} \right\rceil \leq \delta_k + \delta_{k+1} \leq \left\lceil \frac{2w}{2^{n-m}} \right\rceil.$$

Again, the upper and lower bounds are either identical or consecutive positive integers, so

$$\delta_k + \delta_{k+1} \in \left\{ \left\lceil \frac{2w}{2^{n-m}} \right\rceil, \left\lceil \frac{2w}{2^{n-m}} \right\rceil + 1 \right\}. \quad (10)$$

Recall now from the definition of  $\delta_k$  that  $\delta_k\Delta$  is the time length between the  $k$ th and  $k+1$  rising edges of  $s$ , and therefore, it is the length of the  $k$ th interval. Moreover, the length of a (1-0 or 0-1) cycle is  $(\delta_k + \delta_{k+1})\Delta$ . We prove the statements of the theorem in reverse order.

C) The assumption  $L > 2$ , along with [1, eq. (10)], gives  $L = 2^r$  with  $r \geq 2$  implying  $\gcd(w, 2^{n-m}) \leq 2^{n-m-2}$ , and therefore, neither  $w/2^{n-m}$  nor  $2w/2^{n-m}$  is an integer. This means that for  $L > 2$ , inclusions (9) and (10) respectively become

$$\delta_k \in \left\{ \left\lceil \frac{w}{2^{n-m}} \right\rceil, \left\lceil \frac{w}{2^{n-m}} \right\rceil + 1 \right\} \quad (11)$$

and

$$\delta_k + \delta_{k+1} \in \left\{ \left\lceil \frac{2w}{2^{n-m}} \right\rceil, \left\lceil \frac{2w}{2^{n-m}} \right\rceil + 1 \right\}. \quad (12)$$

Moreover, a fundamental continuous-time period  $T_v$  (note that here it is  $T_v = T_p$  because  $L > 1$ , and [1, eq. (23)]) consists of exactly  $L$  consecutive intervals ( $L/2$  are 0-intervals and  $L/2$  are 1-intervals) of  $v$  (see [1, Theorem 4.1]). Assuming that

$$\delta_k = \left\lceil \frac{w}{2^{n-m}} \right\rceil \quad (13)$$

for all  $k$  and using [1, eq. (22)] leads to

$$T_p = L \left\lceil \frac{w}{2^{n-m}} \right\rceil \Delta$$

and so using [1, eq. (10)] and [1, eq. (24)] gives

$$\left\lceil \frac{w}{2^{n-m}} \right\rceil = \frac{w}{2^{n-m}} \quad (14)$$

which is a contradiction because  $w/2^{n-m}$  is not an integer. Similarly, assuming that

$$\delta_k = \left\lceil \frac{w}{2^{n-m}} \right\rceil + 1 \quad (15)$$

for all  $k$  leads to a contradiction for the same reason. Therefore,  $\{\delta_k\}$  takes both values in (11) within every period  $T_v$ .

We prove the rest of part (C) using the fact that  $w/2^{n-m-1}$  is not an integer when  $L > 2$ . Without loss of generality, we assume the initial conditions  $x_0 = 0$  and  $v(0^-) = 0$  to be consistent with Fig. 2. Suppose that all 1-0 cycles have length equal to

$$(\delta_{2j-1} + \delta_{2j})\Delta = \left\lceil \frac{2w}{2^{n-m}} \right\rceil \Delta \quad (16)$$

for all  $j$ . Then, we have

$$T_p = \sum_{j=1}^{L/2} (\delta_{2j-1} + \delta_{2j})\Delta = \frac{L}{2} \left[ \frac{2w}{2^{n-m}} \right] \Delta \quad (17)$$

which using [1, eq. (10)] and [1, eq. (24)] again results in the contradiction

$$\left[ \frac{2w}{2^{n-m}} \right] = \frac{2w}{2^{n-m}} \quad (18)$$

since  $2w/2^{n-m}$  is not an integer. The assumption that 1–0 cycles have length equal to

$$(\delta_{2j-1} + \delta_{2j})\Delta = \left( \left[ \frac{2w}{2^{n-m}} \right] + 1 \right) \Delta \quad (19)$$

for all  $j$  leads to a contradiction for similar reasons.

The proof that the lengths  $(\delta_{2j} + \delta_{2j+1})\Delta$  of 0–1 cycles take both values in (5) within a fundamental continuous-time period  $T_v$  is almost identical. In this case, we consider the fundamental continuous-time period from  $t = \delta_1\Delta$  to  $t = T_v + \delta_1\Delta$  and use

$$T_p = \sum_{j=1}^{L/2} (\delta_{2j} + \delta_{2j+1})\Delta. \quad (20)$$

This concludes the proof of part (C).

B) Since  $\gcd(w, 2^{n-m}) = 2^{n-m-1}$ , inclusion (10) simplifies to the equality  $\delta_k + \delta_{k+1} = w/2^{n-m-1}$ , and so all cycles (1–0 and 0–1) of  $v$  have length equal to

$$(\delta_k + \delta_{k+1})\Delta = \frac{w}{2^{n-m-1}} \Delta \quad (21)$$

which is also equal to  $T_v$  since  $L = 2$ . Once more,  $\gcd(w, 2^{n-m}) = 2^{n-m-1}$  implies that  $w/2^{n-m}$  is not an integer, and using the steps in the proof of part (C), we can show that both values

$$\left[ \frac{w}{2^{n-m}} \right] \quad \text{and} \quad \left[ \frac{w}{2^{n-m}} \right] + 1$$

are taken by sequence  $\{\delta_k\}$ , and using (21), we derive the duty cycle of  $v$  to be

$$D_c = \frac{\delta_1}{\delta_1 + \delta_2} = \left[ \frac{w}{2^{n-m}} \right] \frac{2^{n-m-1}}{w}$$

for the initial values stated in the theorem.

A) Since  $w$  is a multiple of  $2^{n-m}$ , it is  $\delta_k = w/2^{n-m}$  for all  $k = 1, 2, \dots$  ■

*Corollary 3.1:* Let  $w \geq 2^{n-m}$  and  $L > 2$ . Then, every fundamental continuous-time period  $T_v$  starting at the beginning of a 1–0 cycle<sup>8</sup> consists of exactly

$$\rho = \frac{w \bmod 2^{n-m-1}}{\gcd(w, 2^{n-m})} \quad (22)$$

1–0 cycles of length equal to

$$\left( \left[ \frac{2w}{2^{n-m}} \right] + 1 \right) \Delta$$

<sup>8</sup>Like the one from  $t = 0$  to  $t = T_v$  in Fig. 2.

and  $L/2 - \rho$  ones of length equal to

$$\left[ \frac{2w}{2^{n-m}} \right] \Delta.$$

*Proof:* From [1, Corollary 5.3], we know that such a fundamental continuous-time period consists of exactly  $L/2$  1–0 cycles. Then, from part (C) of Theorem 3.1, we have

$$T_v = \rho \left( \left[ \frac{2w}{2^{n-m}} \right] + 1 \right) \Delta + \left( \frac{L}{2} - \rho \right) \left[ \frac{2w}{2^{n-m}} \right] \Delta \quad (23)$$

for some integer  $\rho$ . Using [1, eq. (34)], (23) implies that

$$\rho = \frac{2^{n-m-1}}{\gcd(w, 2^{n-m})} \left( \frac{w}{2^{n-m-1}} - \left[ \frac{w}{2^{n-m-1}} \right] \right). \quad (24)$$

Applying Fact 2 in the Appendix leads to (22). Note that the right-hand side of (22) is always a nonnegative integer. ■

Consider [1, Example 2.1] and [1, Example 2.3] with  $n = 4, m = 2$  and  $w = 7$  and  $w = 15$ , respectively. In both cases it, is  $L = 4$ , and their fundamental continuous-time periods starting at  $t = 0$  have one short and one long 1-0 cycle (as shown in [1, Fig. 3(g)] and [1, Fig. 5(g)]) exactly as predicted by Corollary 3.1, since  $\rho = L/2 - \rho = 1$ . In many cases, the cycles composing the fundamental continuous-time period are all identical except one that is of different size, as illustrated in [5]. This, however, is not true in general, e.g.,  $n = 6, m = 2$  and  $w = 27$  imply  $\rho = 3$  long and  $L/2 - \rho = 5$  short 1-0 cycles for the fundamental continuous-time period starting at  $t = 0$ .

### B. Timing of Pulses and Cycles in $v$

In Section III-A we studied the cycle-to-cycle timing irregularities. Here, we examine the timing irregularities with respect to continuous time  $t$  and derive time windows within which the rising and falling edges of the pulses in  $v$  lie.

From Theorem 3.1, we know that when  $2^{n-m} \leq w < 2^n$  and  $L = 1$ , the output  $v$  is a perfect 50% duty-cycle square wave. Moreover, from [1, Corollary 5.1], we know the frequency  $f = 2^{n-1} f_{\text{clk}}/w$  of the square wave, and we know that the first pulse starts at  $t = 0$  assuming that  $x_0 = 0$  and the D-FF is reset at  $t = 0^-$ . Therefore, for this case, there is nothing more to say.

On the other hand, the case of  $w < 2^{n-m}$  results in highly irregular waveforms (see comments in the beginning of the section).

Therefore, in this section, we assume that  $2^{n-m} \leq w < 2^n$  and  $L > 1$ .

The time sequences  $t_j, j = 1, 2, \dots$ , and  $\tau_j, j = 1, 2, \dots$ , defined in [1, Sec. 2.1] correspond to the rising and following edges of the pulses in the output signal  $v$ . Based on the definition of  $\delta_k$ 's, and with the convention that  $t_0 = 0$ , we have<sup>9</sup>

$$t_j = \Delta \sum_{k=1}^{2j-2} \delta_k \quad (25)$$

and

$$\tau_j = t_j + \Delta \delta_{2j-1}. \quad (26)$$

<sup>9</sup>As before, we assume  $x_0 = 0$  and initially reset D-FF.

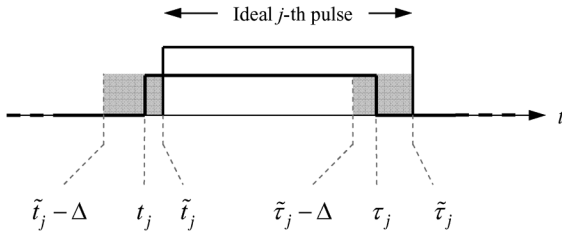


Fig. 3. Timing of the  $j$ th pulse in  $v(t)$  and the  $j$ th pulse in the ideal square wave of frequency  $f_{av}$  when  $2^{n-m} \leq w < 2^n$  and  $L > 1$ .

for  $j = 1, 2, 3, \dots$ . Using (8), which is valid here because of our assumptions,  $t_j$  and  $\tau_j$  are expressed as

$$t_j = \left\lceil \frac{(2j-2)w}{2^{n-m}} \right\rceil \Delta \quad (27)$$

and

$$\tau_j = \left\lceil \frac{(2j-1)w}{2^{n-m}} \right\rceil \Delta. \quad (28)$$

From [1, eq. (34)] and our assumptions, the fundamental continuous-time period of  $v$  can be expressed as

$$T_v = \frac{w}{2^{n-m}} \Delta L \quad (29)$$

and because of  $L > 1$ , it contains  $L/2$  cycles of  $v$  (see also [1, Corollary 5.3]), which is also confirmed by the equality  $t_{L/2+1} = T_v$ . In addition, our assumptions and [1, eq. (42)] imply that the average frequency  $f_{av}$  is the  $N_{av} = L/2$  harmonic of the fundamental frequency  $f_{vf} = 1/T_v$  of the output. Fig. 2 illustrates the timing of the waveform as described above.

Now, we compare the timing of  $v$  to that of the ideal 50% duty-cycle periodic square wave of frequency  $f_{av}$ , whose first rising edge coincides with that of  $v$ . Since there are  $L/2$  pulses within the period  $T_v$ , the rising edge of the  $j$ th pulse of the ideal signal is at

$$\tilde{t}_j = \frac{(2j-2)w}{2^{n-m}} \Delta \quad (30)$$

and the falling edge is at

$$\tilde{\tau}_j = \frac{(2j-1)w}{2^{n-m}} \Delta. \quad (31)$$

Therefore, for all  $j = 1, 2, \dots$ , it is

$$\frac{t_j}{\Delta} = \left\lceil \frac{\tilde{t}_j}{\Delta} \right\rceil \quad \text{and} \quad \frac{\tau_j}{\Delta} = \left\lceil \frac{\tilde{\tau}_j}{\Delta} \right\rceil \quad (32)$$

which imply the following bounds of  $t_j$  and  $\tau_j$ :

$$\tilde{t}_j - \Delta < t_j \leq \tilde{t}_j \quad (33)$$

and

$$\tilde{\tau}_j - \Delta < \tau_j \leq \tilde{\tau}_j. \quad (34)$$

The timings of the  $j$ th pulse in  $v$  and that of the  $j$ th pulse in the ideal square wave are shown in Fig. 3.

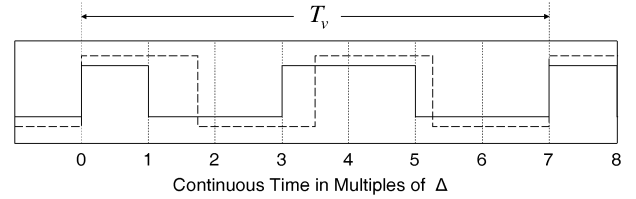


Fig. 4.  $v(t)$  and the ideal square wave of frequency  $f_{av}$  when  $n = 4$ ,  $m = 2$ , and  $w = 7$ . (Solid line)  $v(t)$ . (Dashed line) Ideal square wave.

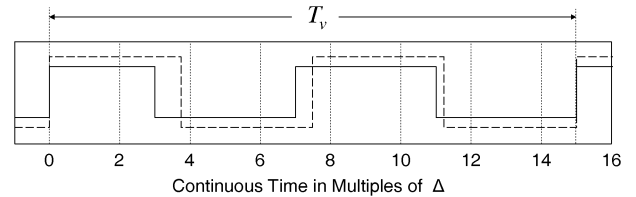


Fig. 5.  $v(t)$  and the ideal square wave of frequency  $f_{av}$  when  $n = 4$ ,  $m = 2$ , and  $w = 15$ . (Solid line)  $v(t)$ . (Dashed line) Ideal square wave.

Note that the rising and falling edges of the  $j$ th pulse in  $v$  appear before or simultaneously to the corresponding ones of the  $j$ th pulse of the ideal square wave. The time offset is less than  $\Delta$ . This provides us with a coarse bound on the deterministic jitter of  $v(t)$ .

*Example 3.3:* The output  $v(t)$  and the ideal square wave of frequency  $f_{av}$  are shown in Fig. 4 for the case of [1, Example 3.1], i.e.,  $n = 4$ ,  $m = 2$ , and  $w = 7$ .

*Example 3.4:* The output  $v(t)$  and the ideal square wave of frequency  $f_{av}$  are shown in Fig. 5 for the case of [1, Example 3.3], i.e.,  $n = 4$ ,  $m = 2$ , and  $w = 15$ .

In most cases with  $2^{n-m} \leq w < 2^n$  and  $L > 1$ , it is true (but note a rule) that the larger the value of  $w$ , the better the timing matching between  $v(t)$  and the ideal square wave (percentage-wise with respect to the length of the period).

*Remark:* From Theorem 3.1 and its proof, we know that every 0 or 1 interval of  $v(t)$  is of length equal to or greater than

$$T_{\min} = \left\lceil \frac{w}{2^{n-m}} \right\rceil \Delta. \quad (35)$$

Therefore, if the FA is used to clock a (synchronous) digital circuit, then the designer should arrange so that  $T_{\min}$  is sufficiently long for all signals to settle. In this case, the digital circuit will appropriately operate at the average clock frequency  $f_{av}$  [16]. Note that (35) is valid for all values of  $L$  as long as  $2^{n-m} \leq w < 2^n$  because of (9).

#### IV. OUTPUT DETERMINISTIC JITTER

The results of the previous section allow us to derive analytic expressions of the output signal's deterministic jitter. Throughout this section, we consider the *rising* edges of the output signal  $v$  appearing at  $t_j$ ,  $j = 1, 2, 3, \dots$ , and all jitter derivations are based on them. One can easily follow the same steps for the falling edges as well. Throughout the paper, "jitter" means *deterministic* jitter.

A time-shifted version of the ideal 50% duty-cycle periodic square wave of frequency  $f_{av} = 1/T_{av}$  is used as a reference

to derive the *accumulated jitter* of  $v$ . When  $w \geq 2^{n-m}$ , [1, eq. (36)] gives

$$T_{av} = \frac{w}{2^{n-m-1}} \Delta. \tag{36}$$

Note that parts (A) and (B) of Theorem 3.1 imply that when  $L = 1$  or  $L = 2$ , the jitter is zero because  $v$  is a juxtaposition of identical cycles; therefore, we can exclude these cases from the calculations that follow. Part (C) of the same theorem implies that jitter is nonzero when  $L > 2$ .

Moreover, from [1, Corollary 5.3], we know that when  $L > 1$ , there are exactly  $L/2$  cycles of  $v$  per fundamental continuous-time period  $T_v$  of it. Therefore,  $L/2$  consecutive cycles of  $v$  provide us all the information we need to derive the value of jitter metrics.

Finally, as discussed in the previous sections, as well as in [1], the output waveform  $v$  is very irregular for most values of the frequency control word  $w$  when  $w < 2^{n-m}$ . With the above comments in mind, the following metrics can be used to quantify the deterministic jitter when  $w \geq 2^{n-m}$  and  $L > 2$ .

- *Absolute Jitter:*

$$J_A = \max_{j=1,2,\dots,L/2} |(t_{j+1} - t_j) - T_{av}|. \tag{37}$$

- *Absolute Cycle-to-Cycle Jitter:*

$$J_{AC2C} = \max_{j=1,2,\dots,L/2} |(t_{j+2} - t_{j+1}) - (t_{j+1} - t_j)|. \tag{38}$$

- *Accumulated Jitter:*

$$J_{ACCU} = \min_{t_{of} \in [0, \Delta]} \left( \max_{j=1,2,\dots,L/2} |t_j - \tilde{t}_j + t_{of}| \right). \tag{39}$$

- *Cycle Average Jitter:*

$$J_{CA} = \sqrt{\frac{2}{L} \sum_{j=1,2,\dots,L/2} ((t_{j+1} - t_j) - T_{av})^2}. \tag{40}$$

- *Cycle-to-Cycle Average Jitter:*

$$J_{C2CA} = \sqrt{\frac{2}{L} \sum_{j=1,2,\dots,L/2} ((t_{j+2} - t_{j+1}) - (t_{j+1} - t_j))^2}. \tag{41}$$

The following lemma provides analytic expressions of the above jitter metrics of  $v$ .

*Lemma 4.1:* When  $w \geq 2^{n-m}$  and  $L \leq 2$ , all jitter metrics (37)–(41) are zero. When  $w \geq 2^{n-m}$  and  $L > 2$ , the jitter metrics (37)–(41), respectively, take the explicit expressions

$$J_A = \frac{\max\{\tilde{w}, 2^{n-m-1} - \tilde{w}\}}{2^{n-m-1}} \Delta \tag{42}$$

$$J_{AC2C} = \Delta \tag{43}$$

$$J_{ACCU} = \frac{2^{n-m-r-1} - 1}{2^{n-m-r}} \Delta \tag{44}$$

$$J_{CA} = \frac{\sqrt{\tilde{w}(2^{n-m-1} - \tilde{w})}}{2^{n-m-1}} \Delta \tag{45}$$

$$J_{C2CA} = \sqrt{\frac{\min\{\tilde{w}, 2^{n-m-1} - \tilde{w}\}}{2^{n-m-2}}} \Delta \tag{46}$$

where the nonnegative integer  $r$  is defined by  $2^r = \text{gcd}(w, 2^{n-m-1})$ , and  $\tilde{w} \triangleq w \bmod 2^{n-m-1}$ .

*Proof:* The case of  $L \leq 2$  is trivial and results directly from parts A) and B) of Theorem 3.1. For the case of  $L > 2$ , we have:

*Equation (42):* Part (C) of Theorem 3.1 implies that within every continuous-time fundamental period,  $t_{j+1} - t_j$  takes both values in (5) and only them. Applying the definition of  $J_A$  and replacing (36), we have

$$\frac{J_A}{\Delta} = \max \left\{ \frac{w}{2^{n-m-1}} - \left\lfloor \frac{w}{2^{n-m-1}} \right\rfloor, \left\lfloor \frac{w}{2^{n-m-1}} \right\rfloor + 1 - \frac{w}{2^{n-m-1}} \right\}.$$

Applying Fact 2 in the Appendix and using the definition of  $\tilde{w}$  in Lemma 4.1, we get (42).

*Equation (43):* Again, part (C) of Theorem 3.1 tells us that  $t_{j+1} - t_j$  takes both values in (5) and only them within every period. Therefore, the maximum of  $|(t_{j+2} - t_{j+1}) - (t_{j+1} - t_j)|$  within a period is exactly the difference  $\Delta$  of the two values in (5).

*Equation (44):* The definitions of  $\tilde{t}_j$  and  $t_j$  along with Fact 2 in the Appendix give

$$\begin{aligned} \frac{\tilde{t}_j - t_j}{\Delta} &= \frac{(j-1)w}{2^{n-m-1}} - \left\lfloor \frac{(j-1)w}{2^{n-m-1}} \right\rfloor \\ &= \frac{((j-1)w) \bmod 2^{n-m-1}}{2^{n-m-1}}. \end{aligned} \tag{47}$$

Using the definition of integer  $r$  in Lemma 4.1, we have that  $w = a2^r$  and  $\text{gcd}(a, 2^{n-m-r-1}) = 1$ . Since  $r \leq n - m - 1$ , we can apply the identity

$$(2^r x) \bmod 2^{n-m-1} = 2^r (x \bmod 2^{n-m-r-1})$$

to get

$$\frac{((j-1)w) \bmod 2^{n-m-1}}{2^{n-m-1}} = \frac{((j-1)a) \bmod 2^{n-m-r-1}}{2^{n-m-r-1}}. \tag{48}$$

Combining (47) with (48) and applying Fact 3 in the Appendix, we get that  $(\tilde{t}_j - t_j)/\Delta$  takes all values of the form  $\ell/2^{n-m-r-1}$ ,  $\ell = 0, 1, 2, \dots, 2^{n-m-r-1} - 1$ , within every period  $T_v$ . Therefore, the minimum in (39) is achieved for

$$t_{of} = \frac{2^{n-m-r-1} - 1}{2^{n-m-r}} \Delta \tag{49}$$

leading to (44).

*Equation (45):* Combining Corollary 3.1 with (40) and using the definition of  $\tilde{w}$  directly leads to (45).

*Equation (46):* Define the function

$$\eta(j) = \frac{(t_{j+2} - t_{j+1}) - (t_{j+1} - t_j)}{\Delta}. \tag{50}$$

From (25) and (27), we can express  $\eta(j)$  as

$$\eta(j) = (\delta_{2j+2} + \delta_{2j+1}) - (\delta_{2j} + \delta_{2j-1}) \tag{51}$$

as well as

$$\eta(j) = \left\lfloor \frac{(j+1)w}{2^{n-m-1}} \right\rfloor - 2 \left\lfloor \frac{jw}{2^{n-m-1}} \right\rfloor + \left\lfloor \frac{(j-1)w}{2^{n-m-1}} \right\rfloor. \tag{52}$$

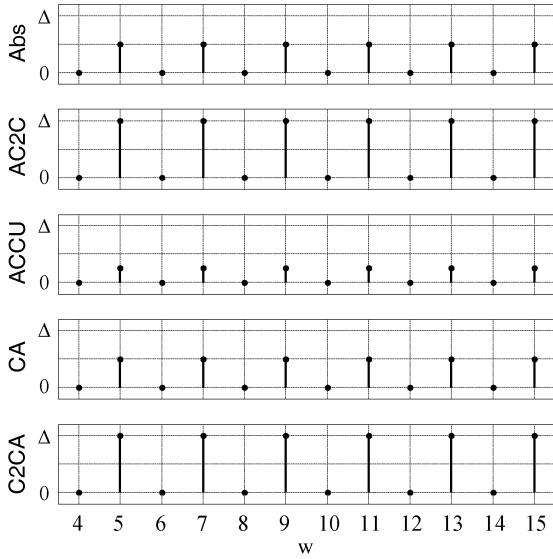


Fig. 6. Jitter metrics  $J_A, J_{AC2C}, J_{ACCU}, J_{CA},$  and  $J_{C2CA}$  when  $n = 4, m = 2,$  and  $w = 2^{n-m}, \dots, 2^n - 1.$

Because of part (C) of Theorem 3.1 and inclusion (12), we have that

$$(\delta_{j+1} + \delta_j) - (\delta_{i+1} + \delta_i) \in \{-1, 0, 1\} \quad (53)$$

for all indices  $i, j \geq 1,$  which gives

$$\eta(j) \in \{-1, 0, 1\} \quad (54)$$

and

$$\sum_{\ell=i}^j \eta(\ell) \in \{-1, 0, 1\} \quad (55)$$

for all  $j \geq i.$  We notice that replacing  $w$  with  $w \bmod 2^{n-m-1}$  in (51) does not change the value of  $\eta(j),$  and so we can assume that  $0 \leq w < 2^{n-m-1}.$  From this, we conclude that the first nonzero value of the sequence  $\eta(j), j = 1, 2, 3, \dots,$  is 1.

Combining (53) with (55), we conclude that the *nonzero* terms of the sequence  $\eta(j)$  form the alternating subsequence  $1, -1, 1, -1, 1, \dots$  whose first term is 1.

In addition, since  $\eta(j)$  is  $L/2$  periodic, the number of 1's must equal the number of -1's in the vector  $(\eta(1), \eta(2), \dots, \eta(L/2)).$  Therefore, to derive  $J_{C2CA},$  we only need to count the number of 1's in this vector. This is done by observing (52) and concluding that there are  $Lw/2^{n-m}$  1's if  $w < 2^{n-m-2}, L/4$  1's if  $w = 2^{n-m-2},$  and  $L(2^{n-m-1} - w)/2^{n-m}$  1's if  $2^{n-m-2} < w < 2^{n-m-1}.$  ■

*Example 4.1:* The different metrics of jitter of the FA with  $n = 4, m = 2,$  and  $w = 2^{n-m}, \dots, 2^n - 1$  are numerically calculated using (42)–(46) and presented in Fig. 6. Note that  $L = 4/\text{gcd}(w, 4)$  and so even values of  $w$  imply  $L = 1$  or  $L = 2$  and therefore zero jitter. The graphs indicate a period of 2 with respect to  $w$  (2 is the smallest value of  $\text{gcd}(w, 4),$  implying zero jitter).

*Example 4.2:* The values of the jitter metrics for the FA with  $n = 8, m = 4,$  and  $w = 2^{n-m}, \dots, 2^n - 1$  are numerically calculated using (37)–(41) and are shown in Fig. 7. Note that  $L = 16/\text{gcd}(w, 16),$  and so the values of  $w$  that are multiples

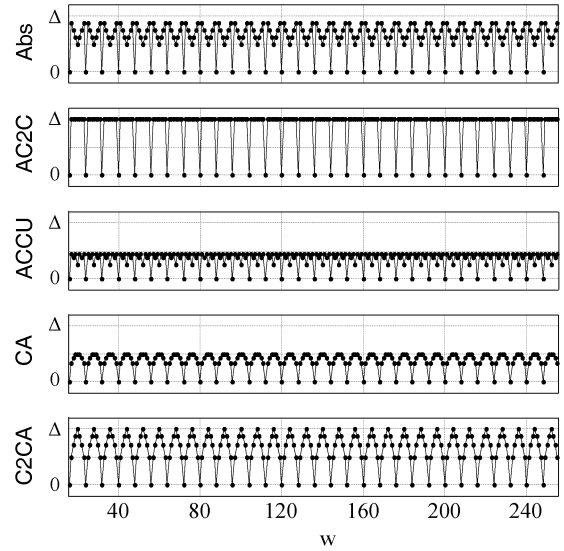


Fig. 7. Jitter metrics  $J_A, J_{AC2C}, J_{ACCU}, J_{CA},$  and  $J_{C2CA}$  when  $n = 8, m = 4,$  and  $w = 2^{n-m}, \dots, 2^n - 1.$

of 8, 16, 32, etc., imply  $L = 1$  or  $L = 2$  and therefore zero jitter. Here, the graphs indicate a period of 8 with respect to  $w$  (note that 8 is the smallest value of  $\text{gcd}(w, 16),$  implying zero jitter).

#### V. OUTPUT SPECTRUM SIGNAL-COMPONENTS POWER

Using the results of the previous sections, we derive the following information about the spectrum of the FA: 1) the average voltage; 2) the average power; 3) the dc power; and 4) the power of the signal component at  $f_{av}$  ( $N_{av} = L/2$  harmonic when  $L > 1$ ) and its dominance in the spectrum.

Theorem 3.1 reveals the exact waveform of  $v(t)$  when  $2^{n-m} \leq w$  and  $L = 1$  or  $L = 2;$  therefore, in this case, the spectrum is known exactly.

**In this section, we assume that  $2^{n-m} \leq w < 2^n$  and  $L > 1.$**

Since signal  $v$  is  $T_v$  periodic, it can be expanded as a Fourier series in the form

$$v(t) = \bar{v} + \sum_{j=1}^{\infty} \left( \alpha_j \cos\left(\frac{2\pi j}{T_v}t\right) + \beta_j \sin\left(\frac{2\pi j}{T_v}t\right) \right) \quad (56)$$

where

$$\alpha_j = \frac{2}{T_v} \int_0^{T_v} v(\sigma) \cos\left(\frac{2\pi j}{T_v}\sigma\right) d\sigma \quad (57)$$

and

$$\beta_j = \frac{2}{T_v} \int_0^{T_v} v(\sigma) \sin\left(\frac{2\pi j}{T_v}\sigma\right) d\sigma \quad (58)$$

for  $j = 1, 2, 3, \dots,$  and  $\bar{v}$  is the average value of  $v.$  Recall also Parseval's identity [42]

$$\frac{1}{T_v} \int_0^{T_v} v^2(t) dt = \bar{v}^2 + \frac{1}{2} \sum_{j=1}^{\infty} (\alpha_j^2 + \beta_j^2). \quad (59)$$

The *output average voltage*  $\bar{v}$  within a time interval  $T_v$  is equal to the ratio  $T_1/T_v,$  where  $T_1$  is the total time length within the interval  $T_v,$  in which  $v(t) = 1.$  From [1, Corollary 5.3],

we know that there are  $L/2$  cycles per fundamental continuous-time period  $T_v$ , and using the definitions of  $t_j$  and  $\tau_j$ , we have that

$$T_1 = \sum_{j=1}^{L/2} (\tau_j - t_j). \quad (60)$$

Replacing (27) and (28) in (60) and setting  $g = \gcd(w, 2^{n-m})$ , we get

$$\begin{aligned} T_1 &= \Delta \sum_{j=1}^{L/2} \left[ \frac{2jw - w}{2^{n-m}} \right] - \Delta \sum_{j=1}^{L/2} \left[ \frac{2jw - 2w}{2^{n-m}} \right] \\ &= \Delta \sum_{j=0}^{L/2-1} \left[ \frac{j\frac{w}{g} + \frac{w}{2g}}{\frac{L}{2}} \right] - \Delta \sum_{j=0}^{L/2-1} \left[ \frac{j\frac{w}{g}}{\frac{L}{2}} \right]. \end{aligned}$$

By assumption,  $L/2$  is a positive integer, and the last two sums can be calculated in closed form using identity (78) in the Appendix, giving

$$T_1 = \left[ \frac{w}{2 \gcd(w, 2^{n-m})} \right] \Delta. \quad (61)$$

Now, our assumptions, i.e.,  $2^{n-m} \leq w < 2^n$  and  $L > 1$ , and [1, eq. (34)] give<sup>10</sup>

$$T_v = \frac{w}{\gcd(w, 2^{n-m})} \Delta. \quad (62)$$

In addition,  $L > 1$  implies that there exist a nonnegative integer  $r < n - m$  and an odd positive integer  $a$  such that  $w = 2^r a$ . Since  $\gcd(w, 2^{n-m}) = 2^r$ , it is

$$T_1 = \left[ \frac{a}{2} \right] \Delta \quad \text{and} \quad T_v = a\Delta. \quad (63)$$

Since  $a$  is odd, we have  $[a/2] = (a-1)/2$ , which along with (63) gives

$$T_1 = \frac{T_v}{2} - \frac{\Delta}{2}. \quad (64)$$

Assuming that the output logical values correspond to 0 and 1 amplitude, the output average voltage  $\bar{v}(t) = T_1/T_v$  is<sup>11</sup>

$$\bar{v} = \frac{1}{2} - \frac{\gcd(w, 2^{n-m})}{2w}. \quad (65)$$

The output average power  $P$  is the average power of  $v(t)$  within a time interval  $T_v$ , i.e.,

$$P = \frac{1}{T_v} \int_0^{T_v} v^2(t) dt. \quad (66)$$

Again, assuming that the output logical values correspond to 0 and 1 amplitude, we get

$$P = \bar{v}. \quad (67)$$

The output dc power  $P_0$  is equal to  $\bar{v}^2$ , and using (65), it is expressed as

$$P_0 = \frac{1}{4} \left( 1 - \frac{\gcd(w, 2^{n-m})}{w} \right)^2. \quad (68)$$

*Power of the  $L/2$  harmonic  $P_{L/2}$ .* Note that our assumption  $L > 1$  implies that  $N_{\text{av}} = L/2$  (see [1, Corollary 5.3]), and so the average frequency  $f_{\text{av}}$  is the  $L/2$  harmonic of the fundamental frequency  $f_{v_j}$  of  $v$ .

Based on the discussion in Section III-B and Figs. 3–5, we can conclude that the major contribution to the power of the  $L/2$  harmonic is due to the  $\sin(\pi \ell t/T_v)$  term in the Fourier series decomposition, since its cycles strongly overlap with those of the ideal waveform. Therefore, from (56) to (59), a lower bound of  $P_{L/2}$  is

$$P_{L/2} \geq \frac{1}{2} (\beta_{L/2})^2 \quad (69)$$

where

$$\beta_{L/2} = \frac{2}{T_v} \int_0^{T_v} v(\sigma) \sin\left(\frac{2\pi L}{T_v} \frac{\sigma}{2}\right) d\sigma. \quad (70)$$

Observing Fig. 2 and following the discussion in Section III-B, we write

$$\beta_{L/2} = \frac{2}{T_v} \sum_{j=1}^{L/2} \int_{t_j}^{\tau_j} \sin\left(\frac{2\pi L}{T_v} \frac{\sigma}{2}\right) d\sigma \quad (71)$$

which, using (29)–(31), gives

$$\begin{aligned} \beta_{L/2} &= \frac{2}{\pi L} \sum_{j=1}^{L/2} \left( \cos\left(\frac{\pi L}{T_v} (\tau_j - \tilde{\tau}_j)\right) \right. \\ &\quad \left. + \cos\left(\frac{\pi L}{T_v} (t_j - \tilde{t}_j)\right) \right). \quad (72) \end{aligned}$$

From (33) and (34), we have that  $|\tau_j - \tilde{\tau}_j| < \Delta$  and  $|t_j - \tilde{t}_j| < \Delta$ , which along with (29) provide the lower bound

$$\beta_{L/2} > \frac{2}{\pi} \cos\left(\frac{2^{n-m}\pi}{w}\right) \quad (73)$$

which is valid and useful when  $w \geq 2^{n-m+1}$ . Another lower bound is given by

$$\beta_{L/2} > \frac{2}{\pi} - \frac{2^{n-m-1}}{w}. \quad (74)$$

It is valid for  $w > 2^{n-m}\pi$ , and it is derived in Lemma 8.2 in the Appendix.

The lower bound (74) is tighter than (73) for small values of  $w$  (see Fig. 8). In addition, note that both expressions in the right sides of (73) and (74) only depend on the ratio  $2^{n-m}/w$ .

A similar procedure can provide us with an upper bound of  $P_{L/2}$ , as well as lower and upper bounds of the power of other harmonics.

<sup>10</sup>Compare (29) with (62).

<sup>11</sup>The quantities are dimensionless.

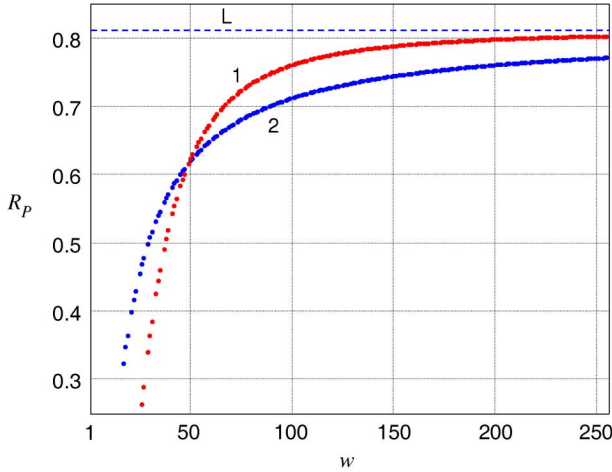


Fig. 8. Lower bounds of  $R_P$  for  $n = 8$  and  $m = 5$ . Curves 1 and 2 correspond to (73) and (74), respectively. The dashed line  $L$  corresponds to the value of  $R_P$  in the case of ideal 50% duty-cycle square wave.

### A. Dominance of the $L/2$ Harmonic

It is important to know what percentage of the total power of  $v(t)$  is due to the  $L/2$  harmonic, i.e., the frequency component at  $f_{av}$ . This is expressed by calculating the power ratio  $R_P$  of  $P_{L/2}$  over the power of the rest of the harmonics, except the dc, i.e.,

$$R_P \triangleq \frac{P_{L/2}}{P - P_0}. \quad (75)$$

Replacing the values of  $P$  and  $P_0$  from (67) and (68) and that of the lower bound (69) in (75), we get the following lower bound of  $R_P$ :

$$R_P > \frac{2(\beta_{L/2})^2}{1 - \left(\frac{\gcd(w, 2^{n-m})}{w}\right)^2}. \quad (76)$$

*Example 5.1:* The graph in Fig. 8 presents the power ratio  $R_P$  using both lower bounds (73) and (74) for  $\beta_{L/2}$  when  $n = 8$  and  $m = 5$ .

Note that Example 5.1 provides one more indication that the larger the value of  $w$  with respect to  $2^n$ , the “cleaner” the output spectrum may be. Intuitively, this makes sense and agrees with the results in Section III-B because the timing error of the pulses in  $v(t)$  is bounded by  $\Delta$ , and so the larger the average frequency period  $T_{av} = 1/f_{av}$ , the smaller the percentile error  $\Delta/T_{av} = \Delta f_{av}$ . Recall from [1, eq. (36)] that when  $2^{n-m} \leq w < 2^n$ , it is  $f_{av} = 2^{n-m-1}/(w\Delta)$ , and so  $\Delta f_{av} = 2^{n-m-1}/w$ .

## VI. MEASUREMENTS AND SIMULATION OF FA'S OUTPUT SPECTRUM

Section III, and particularly Theorem 3.1, provided information about the timing properties of the output signal  $v(t)$ . The average frequency  $f_{av}$  of  $v(t)$  was derived in [1, Sec. 5], and the continuous-time fundamental period  $T_v$  of it was derived in [1, Sec. 4].

This section connects the above derivations with the spectral properties of  $v(t)$  through a number of observations in a collection of instances of the FA's spectrum. The discussion

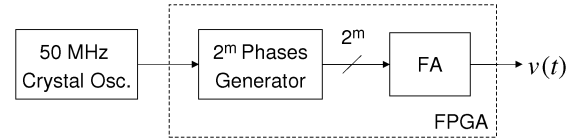


Fig. 9. Setup of the Xilinx Spartan 3E implementation of the FA. The clock frequency of the FA is  $f_{clk} = 50 \text{ MHz}/2^m$ .

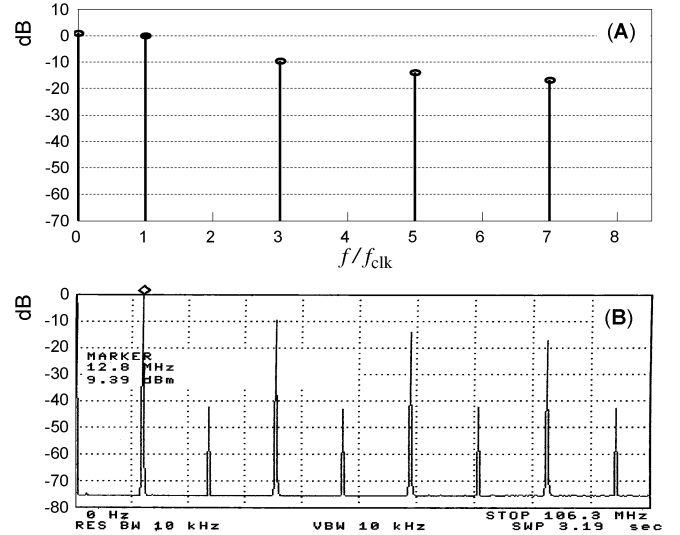


Fig. 10. Output spectrum when  $n = 4$ ,  $m = 2$ , and  $w = 8$ . The average frequency is  $f_{av} = f_{clk}$ . (A) MATLAB-generated spectrum. (B) Measured spectrum of the FPGA implementation with  $f_{clk} = 50 \text{ MHz}/2^m = 12.5 \text{ MHz}$  implying  $f_{av} = 12.5 \text{ MHz}$  (indicated with a rhombus).

here complements the analytical results in Section V. We use both spectral measurements from a Xilinx Spartan 3E field-programmable gate array (FPGA) implementation of the FA (shown in Fig. 9) and spectral estimates numerically derived using MATLAB.

### A. Case: $n = 4$ , $m = 2$

- 1) Consider first the spectra in Fig. 10, where  $n = 4$ ,  $m = 2$ , and  $w = 8$ . The expression in [1, eq. (10)] gives  $L = 1$ , and we also have  $2^{n-m} \leq w$ . Theorem 3.1 tells us that  $v(t)$  is an ideal 50% duty-cycle square wave of period  $T_v = (8/2)\Delta = T$ , i.e.,  $f_{av} = f_{clk}$ . Moreover,  $f_{xy} = f_{vf} = f_{clk}$  since  $N_{av} = 1$ .

As expected, the ideal spectrum in Fig. 10(A) demonstrates the existence (and relative power) of only odd harmonics of  $f_{av}$  plus a dc offset. Instead, the measured spectrum in Fig. 10(B) shows the contribution of even harmonics. Since all of the internal and output frequencies of the FA are identical, the even harmonics must be due to the lack of perfect 50% duty cycle clock or parasitic coupling of some register's bits to the output.

- 2) Now, we examine Fig. 11. Here, it is  $w = 14$ , and so  $L = 2$ ,  $T_v = 7\Delta$ ,  $f_{av} \approx 0.57 f_{clk}$ , and  $N_{av} = 1$ , implying  $f_{av} = f_{vf}$ , i.e.,  $f_{av}$  is the fundamental frequency of the periodic signal  $v(t)$ . Moreover,  $f_{xy} = f_{av}/4$ .

From Theorem 3.1, we know that  $v(t)$  has one pulse per period  $T_v$ , but it is not 50% duty cycle. Fig. 11(A) is in agreement, showing the ideal spectrum with even and

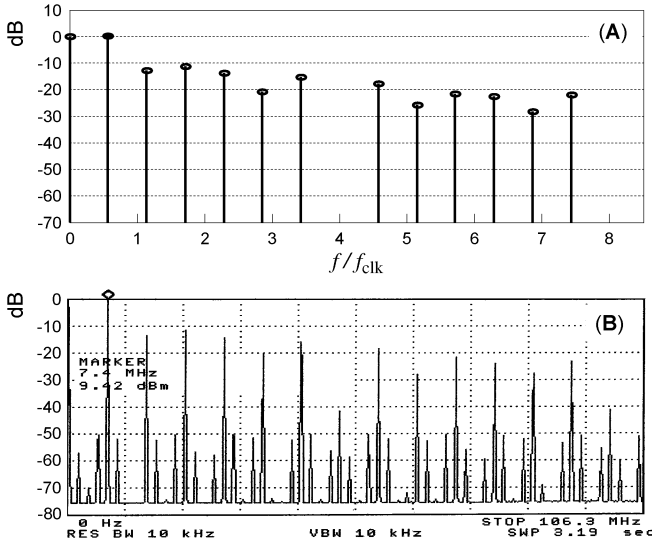


Fig. 11. Output spectrum when  $n = 4$ ,  $m = 2$ , and  $w = 14$ . The average frequency is  $f_{av} \approx 0.57 f_{clk}$ . (A) MATLAB-generated spectrum. (B) Measured spectrum of the FPGA implementation with  $f_{clk} = 50 \text{ MHz}/2^m = 12.5 \text{ MHz}$  implying  $f_{av} \approx 7.14 \text{ MHz}$  (indicated with a rhombus).

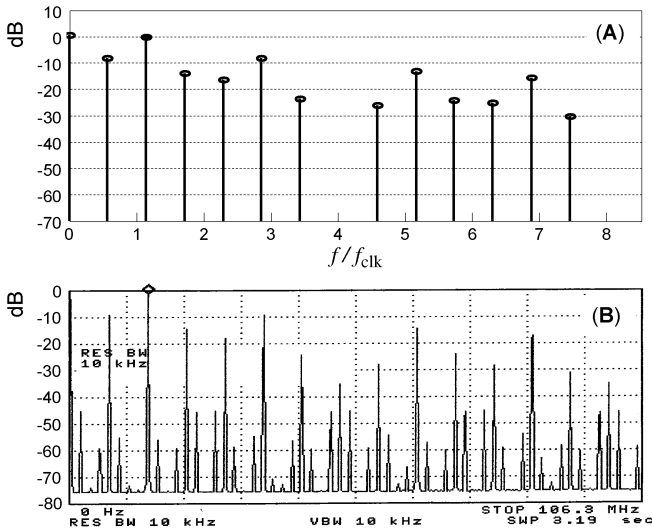


Fig. 12. Output spectrum when  $n = 4$ ,  $m = 2$ , and  $w = 7$ . The average frequency is  $f_{av} \approx 1.14 f_{clk}$ . (A) MATLAB-generated spectrum. (B) Measured spectrum of the FPGA implementation with  $f_{clk} = 50 \text{ MHz}/2^m = 12.5 \text{ MHz}$  implying  $f_{av} \approx 14.29 \text{ MHz}$  (indicated with a rhombus).

odd harmonics of the fundamental frequency  $f_{av}$  in addition to a dc component. Fig. 11(B), however, shows  $f_{av} \approx 7.14 \text{ MHz}$  and its harmonics, along with  $f_{xy} \approx 1.79 \text{ MHz}$  and its harmonics as well, indicating a leakage of the spectrum of the internal states  $x_k, y_k$  to the output or the impact of lack of perfect 50% duty cycle of the driving clock.

3) The spectra of  $v(t)$  for the instances in [1, Examples 2.1–2.3] are shown in Figs. 12–14), respectively. In all three cases,  $w$  is odd, and so  $L$  takes the maximum possible value  $L = 4$ , and [1, Corollary 5.3] implies that there are two pulses of  $v(t)$  per fundamental continuous-time period  $T_v$ .

We observe the following.

a)  $w = 3 < 2^{n-m}$  results in an irregular waveform, as mentioned in Section III and shown in [1, Fig. 4], that

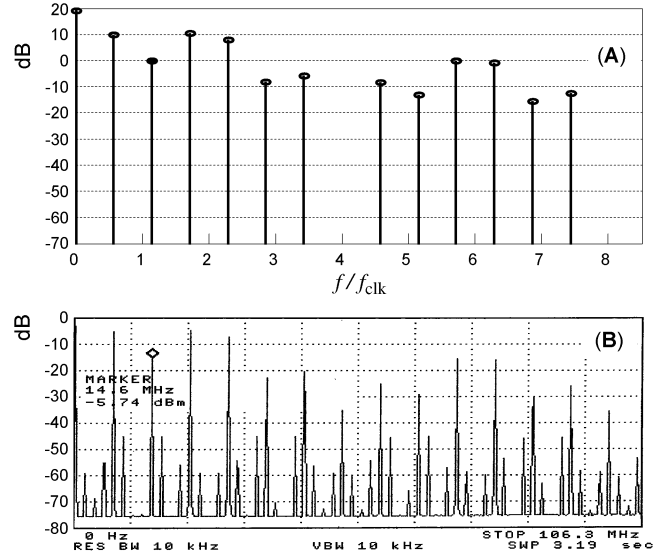


Fig. 13. Output spectrum when  $n = 4$ ,  $m = 2$ , and  $w = 3$ . The average frequency is  $f_{av} = 1.14 f_{clk}$  (same as with  $w = 7$ ). (A) MATLAB-generated spectrum. (B) Measured spectrum of the FPGA implementation with  $f_{clk} = 50 \text{ MHz}/2^m = 12.5 \text{ MHz}$  implying  $f_{av} = 14.29 \text{ MHz}$  (indicated with a rhombus).

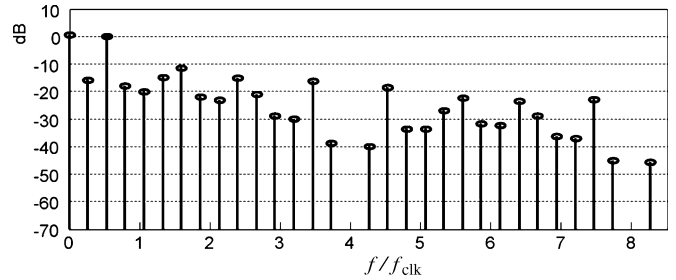


Fig. 14. MATLAB-generated spectrum when  $n = 4$ ,  $m = 2$ , and  $w = 15$ . The average frequency is  $f_{av} \approx 0.53 f_{clk}$ .

(typically for  $w < 2^{n-m}$ ) has very strong nonharmonic frequency components. As shown in Fig. 13, the power of  $f_{av}$  is lower than that of the fundamental  $f_{vf}$  and its third and fourth harmonics ( $f_{av}$  is the second harmonic of the fundamental).

b) Both sets  $w = 7$  and  $w = 3$  result in the same period  $T_v = 7\Delta$  and the same  $f_{av}$  (recall [1, Corollary 5.2(D)]) although  $v(t)$  in the second case is very irregular.

c) In most cases, the larger the odd value of  $w$ , the more dominant the  $f_{av}$  component in the spectrum (among the nonharmonic signals).

3.1) For  $w = 7$ , it is  $f_{av} = 2f_{vf} = 8f_{xy} \approx 1.14 f_{clk}$ , and although the ideal spectrum in Fig. 12(a) only shows  $f_{av}$  and its harmonics, Fig. 12(b) demonstrates the leakage of the spectrum of the internal states  $x_k$  and  $y_k$  to the output ( $f_{av} \approx 14.29 \text{ MHz}$ ,  $f_{vf} \approx 7.14 \text{ MHz}$  and  $f_{xy} \approx 1.79 \text{ MHz}$ ) or possibly the impact of lack of perfect 50% duty cycle of the driving clock.

3.2) For  $w = 3$ , we also have  $f_{av} = 2f_{vf} = 8f_{xy} \approx 1.14 f_{clk}$ , which is exactly as in case (3ci). Similarly, Fig. 13(a) shows the ideal spectrum with  $f_{av}$  and its harmonics,

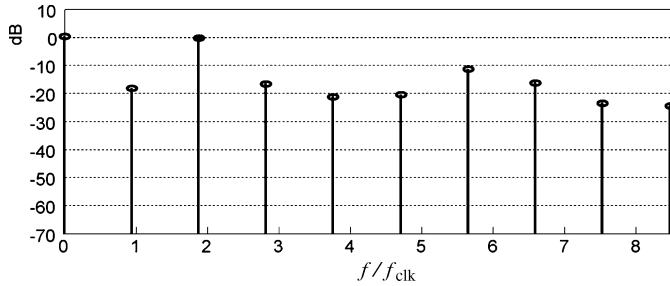


Fig. 15. MATLAB-generated spectrum when  $n = 8$ ,  $m = 4$ , and  $w = 68$ . The average frequency is  $f_{av} \approx 1.88 f_{clk}$ .

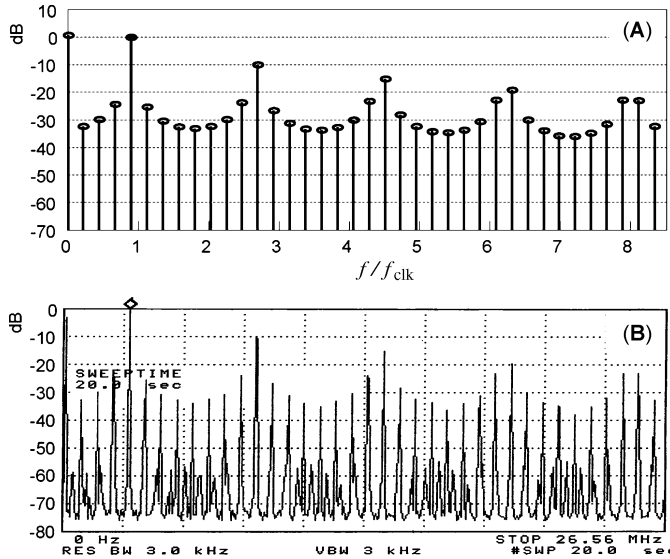


Fig. 16. Output spectrum when  $n = 8$ ,  $m = 4$ , and  $w = 142$ . The average frequency is  $f_{av} \approx 0.90 f_{clk}$ . (A) MATLAB-generated spectrum. (B) Measured spectrum of the FPGA implementation with  $f_{clk} = 50 \text{ MHz}/2^m = 3.125 \text{ MHz}$  implying  $f_{av} \approx 2.82 \text{ MHz}$  (indicated with a rhombus).

whereas Fig. 13(b) shows the presence of  $f_{xy}$  and its harmonics as well. Again, it is  $f_{av} \approx 14.29 \text{ MHz}$ ,  $f_{vf} \approx 7.14 \text{ MHz}$ , and  $f_{xy} \approx 1.79 \text{ MHz}$ .

- 3.3) For  $w = 15$ , we have  $f_{av} = 2f_{vf} = 8f_{xy} \approx 0.53f_{clk}$ . Fig. 14 shows  $f_{av}$  and its harmonics. (Measurements are not presently available for this case.)

#### B. Case: $n = 8$ , $m = 4$

- 1) The ideal spectrum of  $v(t)$  is shown in Fig. 15 for  $w = 68$ . It is  $L = 4$  and  $f_{av} = 2f_{vf} = 32f_{xy} \approx 1.88f_{clk}$ , so  $f_{av}$  is the second harmonic of the fundamental frequency  $f_{vf}$  of  $v(t)$ . The spurious-free dynamic range (SFDR), considering only the nonharmonic signals, is about 16 dB within the frequency range we observe here. (Measurements are not presently available for this case.)
- 2) Figs. 16 and 17 show the spectrum when  $w = 142$ . Here, we have  $L = 8$  and  $f_{av} = 4f_{vf} = 64f_{xy} \approx 0.90f_{clk}$ . Fig. 16(A) confirms that  $f_{av}$  is the fourth harmonic of the fundamental frequency  $f_{vf}$ . Note that the higher value of  $w$  with respect to the previous case results in a higher SFDR equal to 22.8 dB (within the observed frequency range and considering only the nonharmonic signals). Fig. 16(B) shows the measured spectrum. It is  $f_{av} \approx 2.82 \text{ MHz}$ ,  $f_{vf} \approx 0.70 \text{ MHz}$ , and  $f_{xy} \approx 0.044 \text{ MHz}$ .

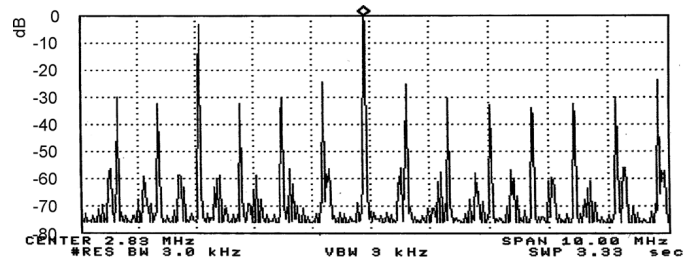


Fig. 17. Zoomed-in measured spectrum of the FPGA implementation with  $n = 8$ ,  $m = 4$ , and  $w = 142$ , centered at  $f_{av} \approx 2.82 \text{ MHz}$  (rhombus).

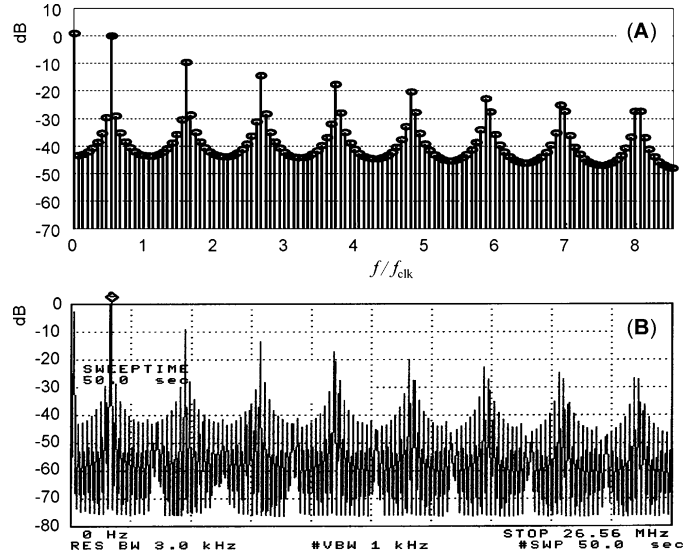


Fig. 18. Output spectrum when  $n = 8$ ,  $m = 4$ , and  $w = 241$ . The average frequency is  $f_{av} \approx 0.53 f_{clk}$ . (A) MATLAB-generated spectrum. (B) Measured spectrum of the FPGA implementation with  $f_{clk} = 50 \text{ MHz}/2^m = 3.125 \text{ MHz}$  implying  $f_{av} \approx 1.66 \text{ MHz}$  (indicated with a rhombus).

Fig. 17 is a zoom-in around  $f_{av}$ , showing more clearly the harmonics of  $f_{xy}$ , which are 16 times denser than those of  $f_{vf}$ .

- 3) Increasing  $w$  to 241 results in the ideal spectrum in Fig. 18(A). SFDR increases to 27.4 dB (within observed frequency range). It is  $L = 16$  and  $f_{av} = 8f_{vf} = 128f_{xy} \approx 0.53f_{clk}$ , so  $f_{av}$  is the eight harmonic of the fundamental frequency  $f_{vf}$ . The odd value of  $w$  here results in higher  $N_{av} = f_{av}/f_{vf} = 8$  compared with that of the previous case with  $w = 142$ . Fig. 18(B) shows the measured spectrum. It is  $f_{av} \approx 1.66 \text{ MHz}$ ,  $f_{vf} \approx 0.21 \text{ MHz}$ , and  $f_{xy} \approx 0.013 \text{ MHz}$ . Fig. 19 is a zoom-in around  $f_{av}$ , showing more clearly the harmonics of  $f_{vf}$ . The graph suggests the presence of the harmonics of  $f_{xy}$ , but due to their high density, it is difficult to identify their position accurately.

#### C. Case: $n = 12$ , $m = 5$

Fig. 20 shows the ideal spectrum of  $v(t)$  when  $n = 12$ ,  $m = 5$ , and  $w = 3151$ . It is  $L = 128$  and  $f_{av} = 64f_{vf} = 2048f_{xy}$ . The SFDR is 32.2 dB (within the observed frequency range and considering only the nonharmonic signals), and  $f_{av} \approx 0.65f_{clk}$ . (Measurements are not presently available for this case.)

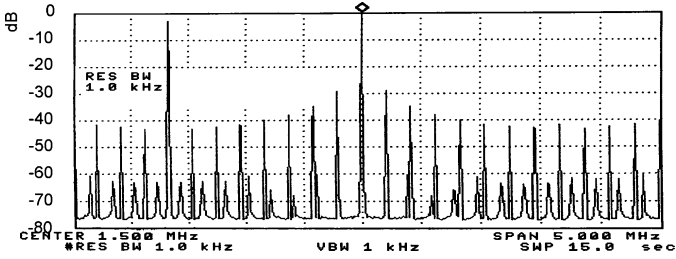


Fig. 19. Zoomed-in measured spectrum of the FPGA implementation with  $n = 8$ ,  $m = 4$ , and  $w = 241$ , centered at  $f_{av} \approx 1.66$  MHz (rhombus).

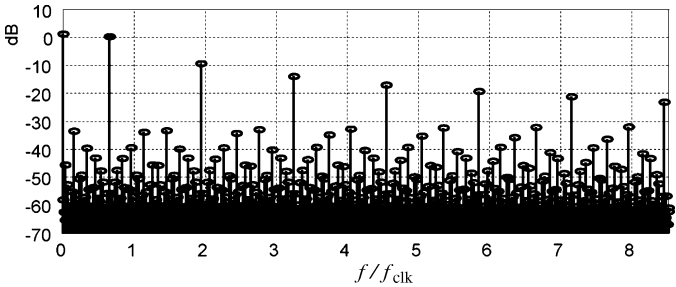


Fig. 20. MATLAB-generated spectrum when  $n = 12$ ,  $m = 5$ , and  $w = 3151$ . The average frequency is  $f_{av} \approx 0.65 f_{clk}$ .

## VII. CONCLUSION

The flying adder frequency synthesizer with register size  $n$  bits,  $2^m$  input (oscillator) phases, and frequency control word  $w$  has been modeled and analyzed mathematically. Several timing and spectral properties of the output signal have been derived.

The FA architecture is compact and fully digital, which makes it attractive for commercial circuit applications that can tolerate its bounded timing irregularities.

For frequency control word  $w \geq 2^{n-m}$ , the timing irregularity of the rising and falling edges of the output signal, as well as that of the duty cycle of its pulses, is always smaller than or equal to  $\Delta = 1/(2^m f_{clk})$ . This must be compared with the period of the average frequency component, which for  $w \geq 2^{n-m}$  is  $w/(2^{n-1} f_{clk})$ .

Exact analytical expressions of the absolute, absolute cycle-to-cycle, accumulated, cycle-average, and cycle-to-cycle average deterministic jitter metrics of the output have been derived. All of them are less than or equal to  $\Delta$  and depend strongly and periodically on the frequency control word  $w$ .

The average-frequency frequency component is dominant in the spectrum of the FA for reasonably large values of  $w$ . The SFDR is typically low in the range of 10–40 dB for most of the values of  $w$ , and the spectrum is typically populated with non-harmonic spurs when  $L > 2$ . The spurs closest to the average frequency  $f_{av}$  component are at frequencies  $f_{av} \pm 1/T_v$ , where  $T_v$  is the fundamental continuous-time period of the output.

Since the FA is simple and compact and offers high period resolution and range adjustment, the above properties make the FA a useful frequency synthesis architecture for digital circuits applications that can tolerate small deterministic jitter. The application of the FA to analog and RF circuits is a subject for future research due to the spurious components in the spectrum.

## APPENDIX

The following *facts* can be found in [43] and other books on discrete mathematics.

*Fact 1*

$$\text{If } x \leq y, \text{ then } [y - x] \leq [y] - [x] \leq \lceil y - x \rceil.$$

*Fact 2*

Letting  $a$  and  $b$  be integers and  $b > 0$ , then

$$\frac{a}{b} - \left\lfloor \frac{a}{b} \right\rfloor = \frac{a \bmod b}{b}. \quad (77)$$

*Fact 3*

Let  $a$  and  $b$  be positive integers and  $\gcd(a, b) = 1$ . Then, the function  $h : \{0, 1, \dots, b-1\} \rightarrow \{0, 1, \dots, b-1\}$  such that  $h(k) = (ka) \bmod b$  is a bijection.

*Lemma 8.1*

Let  $n$  be a nonnegative integer,  $m$  be a positive integer,  $x$  be a real number, and  $d = \gcd(m, n)$ . Then, from [43], we know that

$$\sum_{k=0}^{m-1} \left\lfloor \frac{nk + x}{m} \right\rfloor = d \left\lfloor \frac{x}{d} \right\rfloor + \frac{m-1}{2}n + \frac{d-m}{2}. \quad (78)$$

*Lemma 8.2*

Inequality (74) is valid for  $w > 2^{n-m}\pi$ .

*Proof:* Since  $\pi L \Delta / T_v = 2^{n-m}\pi/w$ , assumption  $w > 2^{n-m}\pi$ , along with (33) and (34), implies that

$$\left| \frac{\pi L}{T_v} (\tilde{\tau}_j - \tau_j) \right| < 1 \quad \text{and} \quad \left| \frac{\pi L}{T_v} (\tilde{t}_j - t_j) \right| < 1$$

and so setting  $\delta = \tilde{\tau}_j - \tau_j$  or  $\delta = \tilde{t}_j - t_j$ , we have

$$\cos \left( \frac{\pi L}{T_v} \delta \right) \geq 1 - \frac{1}{2} \left( \frac{\pi L}{T_v} \delta \right)^2 \geq 1 - \frac{1}{2} \left( \frac{\pi L}{T_v} \delta \right)$$

which using (72) gives

$$\beta_{L/2} \geq \frac{2}{\pi} - \frac{1}{T_v} \sum_{j=1}^{L/2} (\tilde{t}_j + \tilde{\tau}_j - t_j - \tau_j). \quad (79)$$

Using (78) and setting  $g = \gcd(w, 2^{n-m})$ , we derive

$$\sum_{j=1}^{L/2} \tilde{t}_j = \frac{w \Delta L}{2^{n-m+1}} \left( \frac{L}{2} - 1 \right) \quad (80)$$

$$\sum_{j=1}^{L/2} \tilde{\tau}_j = \frac{w \Delta}{2^{n-m}} \frac{L^2}{4} \quad (81)$$

$$\sum_{j=1}^{L/2} t_j = \frac{1}{2} \left( \frac{L}{2} - 1 \right) \left( \frac{w}{g} - 1 \right) \Delta \quad (82)$$

$$\sum_{j=1}^{L/2} \tau_j = \left\lfloor \frac{w}{2g} \right\rfloor \Delta + \frac{1}{2} \left( \frac{L}{2} - 1 \right) \left( \frac{w}{g} - 1 \right) \Delta. \quad (83)$$

Adding (80)–(83) gives

$$\sum_{j=1}^{L/2} (\tilde{t}_j + \tilde{\tau}_j - t_j - \tau_j) = \frac{L-1}{2} \Delta. \quad (84)$$

Note that by assumption it is  $L > 1$ , which implies that  $w/g$  is an odd positive integer and so

$$\frac{w}{2g} - \left\lfloor \frac{w}{2g} \right\rfloor = \frac{1}{2}. \quad (85)$$

Finally, (79), (84), and (85) give

$$\beta_{L/2} \geq \frac{2}{\pi} - \frac{2^{n-m-1}}{w} \frac{L-1}{L} > \frac{2}{\pi} - \frac{2^{n-m-1}}{w}. \quad \blacksquare$$

#### ACKNOWLEDGMENT

The author would like to thank L. Xiu of NovaTek for useful discussions and insightful feedback, W. A. Ling for proofreading the manuscript, Editor-in-Chief Prof. G. Setti and Associate Editor Prof. A. Strollo for their helpful suggestions and their administrative efforts in dealing with this two-part paper, and the anonymous reviewers for their constructive comments.

#### REFERENCES

- [1] P. Sotiriadis, "Theory of Flying-Adder frequency synthesizers—Part I: Modeling, signals periods and output average frequency," *IEEE Trans. Circuits Syst. I, Reg. Papers*, vol. 57, 2010, to be published.
- [2] H. Mair and L. Xiu, "An architecture of high-performance frequency and phase synthesis," *IEEE J. Solid-State Circuits*, vol. 35, no. 6, pp. 835–846, Jun. 2000.
- [3] H. Mair, L. Xiu, and S. A. Fahrenbruch, "Precision frequency and phase synthesis," U.S. Patent 6 329 850, Dec. 11, 2001.
- [4] D. E. Calbaza and Y. Savaria, "A direct digital periodic synthesis circuit," *IEEE J. Solid-State Circuits*, vol. 37, no. 8, pp. 1039–1045, Aug. 2002.
- [5] L. Xiu, "Some open issues associated with the new type of component: Digital-to-frequency converter [Open Column]," *IEEE Circuits Syst. Mag.*, vol. 8, no. 3, pp. 90–94, 3rd Quart., 2008.
- [6] D. Calbaza and Y. Savaria, "A direct digitally delay generator," in *Proc. Int. Circuits Syst.*, Sinaia, Romania, Oct. 2000, vol. 1, pp. 87–90.
- [7] L. Xiu and Z. You, "A 'Flying-Adder' architecture of frequency and phase synthesis with scalability," *IEEE Trans. Very Large Scale Integr. (VLSI) Syst.*, vol. 10, no. 5, pp. 637–649, Oct. 2002.
- [8] L. Xiu and Z. You, "A new frequency synthesis method based on 'Flying-Adder' architecture," *IEEE Trans. Circuits Syst. II, Analog Digit. Signal Process.*, vol. 50, no. 3, pp. 130–134, Mar. 2003.
- [9] L. Xiu, W. Li, J. Meiners, and R. Padakanti, "A novel all digital phase lock loop with software adaptive filter," *IEEE J. Solid-State Circuits*, vol. 39, no. 3, pp. 476–483, Mar. 2004.
- [10] B. Izouggaghen, A. Khous, and Y. Savaria, "Spurs modeling in direct digital period synthesizers related to phase accumulator truncation," in *Proc. ISCAS*, May 2004, vol. 3, pp. 389–392.
- [11] L. Xiu and Z. You, "A 'Flying-Adder' frequency synthesis architecture of reducing VCO stages," *IEEE Trans. Very Large Scale Integr. (VLSI) Syst.*, vol. 13, no. 2, pp. 201–210, Feb. 2005.
- [12] M. E. Salomon, A. Khous, and Y. Savaria, "A complete spurs distribution model for direct digital period synthesizers," in *Proc. ISCAS*, May 2005, vol. 5, pp. 4859–4862.
- [13] B. Pontikakis, H.-T. Bui, F.-R. Boyer, and Y. Savaria, "Precise free-running period synthesizer (FRPS) with process and temperature compensation," in *Proc. IEEE Midwest Symp. Circuits Syst.*, 2007, pp. 1118–1121.
- [14] L. Xiu, "A novel DCXO module for clock synchronization in MPEG2 transport system," *IEEE Trans. Circuits Syst. I, Reg. Papers*, vol. 55, no. 8, pp. 2226–2237, Sep. 2008.
- [15] L. Xiu, "A 'Flying-Adder' based on-chip frequency generator for complex SoC," *IEEE Trans. Circuit Syst. II, Exp. Briefs*, vol. 54, no. 12, pp. 1067–1071, Dec. 2007.
- [16] L. Xiu, "A Flying-Adder PLL technique enabling novel approaches for video/graphic applications," *IEEE Trans. Consum. Electron.*, vol. 54, no. 2, pp. 591–599, May 2008.
- [17] M. E. Salomon, B. Izouggaghen, A. Khous, and Y. Savaria, "Spur model for a fixed-frequency signal to period jitter," *IEEE Trans. Instrum. Meas.*, vol. 57, no. 10, pp. 2320–2328, Oct. 2008.
- [18] L. Xiu, "Flying-Adder on-chip frequency synthesis architecture," in *Proc. IEEE SOC Conf.*, 2008, p. 389.
- [19] C.-W. Huang, P. Gui, and L. Xiu, "A wide-tuning-range and reduced-fractional-spurs synthesizer combining  $\Sigma$ - $\Delta$  fractional-N and integer Flying-Adder techniques," in *Proc. IEEE Int. Symp. Circuits Syst.*, 2009, pp. 1377–1380.
- [20] L. Xiu, C.-W. Huang, and P. Gui, "Simulation study of time-average-frequency based clock signal driving systems with embedded digital-to-analog converters," in *Proc. IEEE SOC Conf.*, 2009, pp. 465–468.
- [21] V. Manassewitsch, *Frequency Synthesizers*, 3rd ed. New York: Wiley, 1987.
- [22] U. L. Rohde, *Microwave and Wireless Synthesizers: Theory and Design*, 1st ed. New York: Wiley-Interscience, 1997.
- [23] W. F. Egan, *Frequency Synthesis by Phase Lock*, 2nd ed. New York: Wiley, 1999.
- [24] V. S. Reinhardt, "Direct digital synthesizers," Hughes Aircraft Co., Space and Commun. Group, Los Angeles, CA, Tech. Rep., Dec. 1985.
- [25] P. Nuytkens and P. Van Broekhoven, "Digital frequency synthesizer," Jun. 12, 1990.
- [26] *Direct Digital Frequency Synthesizers*, V. F. Kroupa, Ed. New York: Wiley-IEEE Press, 1998.
- [27] B. G. Goldberg, *Digital Techniques in Frequency Synthesis*. New York: McGraw-Hill, 1995.
- [28] J. Nieznanski, "An alternative approach to the ROM-less direct digital synthesis," *IEEE J. Solid-State Circuits*, vol. 33, no. 1, pp. 169–170, Jan. 1998.
- [29] K. Shu, E. Sanchez-Sinencio, J. Silva-Martinez, and S. H. K. Embabi, "A 2.4-GHz monolithic fractional-N frequency synthesizer with robust phase-switching prescaler and loop capacitance multiplier," *IEEE J. Solid-State Circuits*, vol. 38, no. 6, pp. 866–874, Jun. 2003.
- [30] P. K. Hanumolu, V. Kratyuk, G.-Y. Weil, and U. Moon, "A sub-pico-second resolution 0.5–1.5 GHz digital-to-phase converter," in *VLSI Symp. Tech Dig.*, Jun. 2006, pp. 75–76.
- [31] D. L. Duttweiler and D. G. Messerschmitt, "Analysis of digitally generated sinusoids with application to A/D and D/A converter testing," *IEEE Trans. Commun.*, vol. COM-26, no. 5, pp. 669–675, May 1978.
- [32] S. Mehrgardt, "Noise spectra of digital sine-generators using the table-lookup method," *IEEE Trans. Acoust., Speech, Signal Process.*, vol. ASSP-31, no. 4, pp. 1037–1039, Aug. 1983.
- [33] D. R. Morgan and A. Aridgides, "Discrete-time distortion analysis of quantized sinusoids," *IEEE Trans. Acoust., Speech, Signal Process.*, vol. ASSP-33, no. 1, pp. 323–326, Feb. 1985.
- [34] J. H. Blythe, "The spectrum of the quantized sinusoid," *GEC J. Res.*, vol. 3, no. 4, pp. 229–242, 1985.
- [35] H. T. Nicholas and H. Samuelli, "An analysis of the output spectrum of direct digital frequency synthesizers in the presence of phase-accumulator truncation," in *Proc. 41st Annu. Freq. Control Symp.*, 1987, pp. 495–502.
- [36] J. F. Garvey and D. Babitch, "An exact spectral analysis of a number controlled oscillator based synthesizer," in *Proc. IEEE Int. Freq. Control Symp.*, 1990, pp. 511–521.
- [37] J. Vankka and K. Halonen, *Direct Digital Synthesizers: Theory, Design and Applications*. Boston, MA: Kluwer, 2001.
- [38] A. Torosyan and A. N. Wilson, Jr., "Analysis of the output spectrum for direct digital frequency synthesizers in the presence of phase truncation and finite arithmetic precision," in *Proc. 2nd Image Signal Process. Anal. Conf.*, 2001, pp. 458–463.
- [39] F. Curticiăpean and J. Niittylahti, "Exact analysis of spurious signals in direct digital frequency synthesizers due to phase truncation," *Electron. Lett.*, vol. 39, no. 6, pp. 499–501, Mar. 20, 2003.
- [40] S. Cheng, J. R. Jensen, R. E. Wallis, and G. L. Weaver, "Further enhancements to the analysis of spectral purity in the application of practical direct digital synthesis," in *Proc. IEEE Int. Freq. Control Symp. Expo.*, Montreal, QC, Canada, 2004, pp. 462–470.

- [41] A. Torosyan and A. N. Wilson, Jr., "Exact analysis of DDFS spur and SNR due to phase truncation and arbitrary phase-to-amplitude errors," in *Proc. IEEE Int. Freq. Control Symp. Expo.*, Aug. 2005, pp. 50–58.
- [42] E. Titchmarsh, *The Theory of Functions*, 2nd ed. Oxford, U.K.: Oxford Univ. Press, 1939.
- [43] R. L. Graham, D. E. Knuth, and O. Patashnik, *Concrete Mathematics: A Foundation for Computer Science*, 2nd ed. Reading, MA: Addison-Wesley, 1994.



**Paul P. Sotiriadis** (S'99–M'02–SM'09) received the Diploma in electrical and computer engineering from the National Technical University of Athens, Athens, Greece, in 1994, the M.S. degree in electrical engineering from Stanford University, Stanford, CA, in 1996, and the Ph.D. degree in electrical engineering and computer science from the Massachusetts Institute of Technology, Cambridge, in 2002.

In 2002, he was an Assistant Professor of electrical and computer engineering with the Johns Hopkins University, Baltimore, MD. In 2007, he was a Chief

Technology Officer with Apex/Eclipse INC. Shortly after that, he started an electronics research company named Sotekco Electronics LLC, Baltimore. He has led several projects funded by U.S. organizations and has collaborations with industry and national laboratories. He has authored or coauthored over 70 technical papers in IEEE journals and conferences, has one patent and several patents pending, and has contributed chapters to technical books. His research interests include design, optimization, and mathematical modeling of analog and mixed-signal circuits, RF and microwave circuits, advanced frequency synthesis, biomedical instrumentation, and interconnect networks in deep-submicrometer technologies.

Dr. Sotiriadis serves as an Associate Editor of the IEEE TRANSACTIONS ON CIRCUITS AND SYSTEMS II—EXPRESS BRIEFS. He has been a member of the technical committees of several conferences. He regularly reviews for many IEEE Transactions and conferences. He also serves on proposal review panels at the National Science Foundation.